Physica Medica 129 (2025) 104879

Contents lists available at ScienceDirect

Physica Medica

journal homepage: www.elsevier.com/locate/ejmp

Individualized evaluation of the total dose received by radiotherapy patients: Integrating in-field, out-of-field, and imaging doses

Maite Romero-Expósito [a,b,*], Beatriz Sánchez-Nieto [c], Mercedes Riveira-Martin [d,1], Mona Azizi [b,e], Angeliki Gkavonatsiou [a], Isidora Muñoz [c], Ignacio N. López-Martínez [c], Ignacio Espinoza [c], Gabriel Zelada [f], Andrés Córdova-Bernhardt [f], Ola Norrlid [g], Christina Goldkuhl [h], Daniel Molin [i], Francisco Mosquera-Pena Sánchez [j], Antonio López-Medina [j,k], Iuliana Toma-Dasu [b,e], Alexandru Dasu [a,l]

[a] The Skandion Clinic, Uppsala, Sweden
[b] Oncology Pathology Department, Karolinska Institutet, Stockholm, Sweden
[c] Pontificia Universidad Católica de Chile, Instituto de Física, Santiago, Chile
[d] Medical Physics and RP Department, Galicia Sur Health Research Institute, Vigo, Spain
[e] Medical Radiation Physics, Stockholm University, Stockholm, Sweden
[f] Servicio de Radioterapia, Clínica Alemana-Universidad del Desarrollo, Santiago, Chile
[g] Uppsala University Hospital, Uppsala, Sweden
[h] Sahlgrenska University Hospital, Gothenburg, Sweden
[i] Department of Immunology, Genetics and Pathology, Cancer Immunotherapy, Uppsala University, Uppsala, Sweden
[j] Medical Physics and RP Department (GALARIA), University Hospital of Vigo, Meixoeiro Hospital, Vigo, Spain
[k] Instituto de Investigación Sanitaria Galicia Sur, Vigo, Spain
[l] Medical Radiation Sciences, Department of Immunology, Genetics and Pathology, Uppsala University, Uppsala, Sweden

ARTICLE INFO

Keywords:
Imaging doses
RT out-of-field doses
Total doses
Risk assessment

ABSTRACT

Purpose: To propose a methodology for integrating the out-of-field and imaging doses to the in-field dose received by radiotherapy (RT) patients. In addition, the impact of considering the total dose in planning and radiation-induced second malignancies (RISM) risk assessment will be evaluated in several scenarios comprising photon and proton treatments.

Methods: The total dose is the voxel-wise sum of the doses from the different radiation sources (accounting for the radiobiological effectiveness) produced during the whole RT chain. The dose from the plan and imaging procedures were obtained by measurements for a photon prostate treatment and by calculation (combining treatment planning system, analytical models, and Monte Carlo simulations) for two lymphoma treatments, one using photons and the other, protons. Dose distributions, dose volume histograms (DVHs) metrics, mean organ doses, and RISM risks were evaluated for each radiation exposure in each treatment.

Results: In general, the contribution of the imaging doses is low compared to the dose administered during RT treatment, being higher in proton therapy. However, for some organs, for instance testes in the prostate case, the imaging dose becomes higher than the scattered dose from the treatment fields. Plan evaluations revealed shifts in cumulative DVHs with the inclusion of out-of-field and imaging doses, though minimal clinical impact is expected. Risk assessment showed increased estimates with total dose.

Conclusions: The methodology enables accounting for the total dose for optimization of plans and imaging protocols, prospective risk predictions and retrospective epidemiological analyses.

* Corresponding author at: Cancercentrum Karolinska (CCK), Karolinska Sjukhuset i Solna, Visionsgatan 56A, våning 3, 171 76 Stockholm, Sweden.
E-mail address: maite.romero@skandion.se (M. Romero-Expósito).
[1] Department of Radiology, Rehabilitation and Physiotherapy, Medicine School, Complutense University of Madrid, Madrid, Spain.

https://doi.org/10.1016/j.ejmp.2024.104879
Received 15 March 2024; Received in revised form 7 October 2024; Accepted 9 December 2024
Available online 22 December 2024
1120-1797/© 2024 Associazione Italiana di Fisica Medica e Sanitaria. Published by Elsevier Ltd. This is an open access article under the CC BY-NC-ND license (http://creativecommons.org/licenses/by-nc-nd/4.0/).

1. Introduction

The significant improvement in medical therapy and radiation therapy (RT) techniques has resulted in an increasingly improved survival rate for cancer patients. Thus, a high number of long-term cancer survivors is expected with an increased risk of developing treatment-induced side effects, such as cardiovascular disease, cognitive disorders, fertility problems, radiation-induced second malignancies (RISM), and other toxicities [1]. All these long-term effects should be considered during treatment planning and optimisation. In fact, ICRU report no. 83 [2] recommended reporting the dose to the "*remaining volume at risk*" (RVR), defined by the difference between the volume enclosed by the external contour of the patient and that of the target and organs-at-risk. They precisely stated that the dose in this region may be useful in estimating the risk of late effects.

Over the past decades, there has been an increased concern about RISM [3]. In adults, the proportion of second cancers related to RT was estimated at approximately 8 %, with proportions varying from 4 to 24 % for the specific sites considered [4]. In terms of absolute risk, the RISM rate has been estimated to be in the order of 1 % [5]. The expected risk for paediatric patients is higher [6] due to the higher radiosensitivity [7] and longer life-time expectancy. Galloway [8] showed actuarial incidences of RISM of 3 %, 8 %, and 24 % at 10, 20, and 30 years of follow-up, respectively, for children receiving brain and craniospinal irradiation. RISM can appear not only in the high-dose area, but in any part of the body exposed to a low dose, albeit with varying probabilities [9]. In fact, patients are exposed to low doses far from the treatment area. In the context of the RVR, the dose to the patient's entire body will be of interest. Scatter and secondary radiation are produced during the delivery of the primary treatment field, resulting from the interaction of the treatment beam with the elements of the delivery system and the patient. This exposure is referred to as an out-of-field dose or stray dose. In the case of photon RT, the out-of-field dose is due to photons and neutrons (the latter when the linear accelerator operates at energies above 8 MV). In the case of particle therapy, in addition to photons and neutrons, other nuclear fragments can be produced in interactions. The contribution of each type of particle is different among the techniques. This radiation has been extensively studied over the last 20 years in photon- and, more recently, proton therapy [10–12]. However, this is not the complete picture of the low doses received by the patient, as there is an additional component of low dose, namely, the one coming from imaging [13,14].

Concern about the imaging dose has been raised recently due to the widespread use of advanced techniques and their increased application in patients. For instance, in the study of Rehani *et al.* [15], the collected data indicated that overall, 1.33 % of patients undergoing CT exams received radiation doses from multiple CT exams with a cumulative effective dose higher than 100 mSv. Considering the definition of effective dose, this result implies that many organs may exceed the reported 100 mSv. Over the years, imaging techniques for RT have undergone a profound transformation. A protocol involving one CT scan for treatment planning, along with one or two simulation images for setup and an additional one or two portal images at the initiation of specific treatment fractions, has evolved to the current image-guided radiotherapy (IGRT) encompassing a range of imaging procedures for various stages of the treatment: planning, simulation, setup and intra-fraction monitoring [16]. Standard imaging procedures for IGRT are cone-beam computed tomography (CBCT), kilovoltage planar imaging, stereoscopic imaging, and portal imaging. All these procedures allow verifying the correct position of the target structures (or only the positioning of the patient as a whole) before and eventually during the treatment, making it possible to exploit the benefit of dose conformation in intensity-modulated radiotherapy (IMRT), volumetric modulated arc therapy (VMAT), or proton therapy. The cost of a successful treatment is that patients undergo more imaging procedures, increasing the total exposure [14].

Regarding cancer incidences, some analyses have found elevated risks of cancer after exposure to low and moderate doses through CT scans in childhood [17,18]. From the perspective of RT, the AAPM task Group 75 [16] provided dose estimates for various image guidance techniques and recommended strategies for minimizing imaging dose when improving treatment delivery. AAPM TG 180 [19] updated dose data resulting from image acquisition procedures and recommended that imaging dose be considered part of the total dose at the treatment planning stage if the dose from repeated imaging procedures is expected to exceed 5 % of the prescribed target dose. The 2013 Basic Standards Safety Directive ("2013/59/Euratom of 5 December 2013") [20] states that "*any equipment used for interventional radiology and computed tomography and any new equipment used for planning, guiding and verification purposes has a device or a feature informing the practitioner, at the end of the procedure, of relevant parameters for assessing the patient dose*" (Article 60.3). This standard, including CBCT, highlights the relevance of reporting the imaging doses. Furthermore, it is possible to provide a 3D dose calculation that can be superimposed on the dose received by RT. This total dose distribution over the whole patient body becomes indispensable for epidemiological studies on RISM risk among cancer survivors [13].

Therefore, the present work aims to study the methodology for individually evaluating the total dose a patient receives. The individualization will be in terms of the patient-specific evaluation of the dose distributions under the specific exposure conditions over its actual anatomy. A particular emphasis will be placed on integrating the imaging dose into the RT dose, through the experimental evaluation of the whole course of a VMAT prostate treatment. Then, the methodology will be employed for two selected lymphoma treatments: *i)* diffuse large B-cell lymphoma (DLBCL) treated with VMAT and *iii)* classical Hodgkin lymphoma (cHL) treated with protons. A final aim is to analyse the impact of this total dose on both the planning process and the assessment of the RISM risk.

2. Material and methods

2.1. Total dose methodology

The total dose is the sum of the dose received from the treatment itself and from the imaging procedures through the whole RT chain. Ideally, this summation should be conducted on a voxel-by-voxel basis to generate a comprehensive total dose matrix. Thus,

$$H_T = H_{prim} + H_{sec} + H_{imag} \tag{1}$$

Where H_T stands for the total dose, H_{prim} the dose due to the treatment beam, H_{sec} the secondary radiation and, H_{imag}, the dose due to imaging. The different components may refer to different particles and, therefore, the different radiobiological effectiveness has to be taken into account.

At this point, an important remark is needed since the total dose includes both high and low doses, each of which is handled differently. For instance, for low doses, a whole system was designed around the concept of dose equivalent (or equivalent dose in organ), quantity measured in Sv [21]. Photons are considered the reference radiation for biological effects, and absorbed doses (in Gy) and equivalent doses are numerically equal. In the case of neutrons, produced as secondary radiation in all cases, doses are within the low dose range; therefore, the dose equivalent is the appropriate quantity. The case of protons deserves a more detailed consideration. On one hand, in the range of treatment doses, the proton therapy community defines the therapeutic dose by multiplying the absorbed dose by a relative biological effectiveness (RBE) factor equal to 1.1, given in units of Gy(RBE) [22]. On the other hand, in the low dose range, the International Commission on Radiobiological ICRP recommends a radiation weighting factor w_R (based on RBE) of 2 [21]. Our proposal for the methodology is to use a different weighting factor depending on the region. Thus, the 1.1 factor is used

within the in-field area (defined by the 50 % isodose of the treatment), while the 2 factor is used in the out-field area. For the sake of simplicity and consistency along the manuscript, the Sv will be used for all doses.

Fig. 1 depicts the chart of the proposed flow to evaluate equation (1). Firstly, as initial inputs, DICOM data from the treatment planning system (TPS) is considered: *i)* planned dose distribution (*RTDose*), *ii)* technical parameters of the plan (*RTPlan*), *iii)* planning CT (*pCT*), *iv)* segmented structures used in the planning (*RTStruct*), and *v)* set of verification/setup CT and/or CBCT images (*Ximg*). The RT_{Plan} identifies the beam particle, determining how to proceed for the evaluation of H_{prim} and H_{sec}. If the case is a photon plan, the *RTDose* defines H_{prim} but only up to the level of 5 % of the prescribed dose, due to the fact that in the TPS, the implemented model for out-of-field doses fails in accounting for scatter far away from the target and leakage from the linac, resulting in an underestimation of the doses [23,24]. If the plan is a proton plan, the *RTDose* defines H_{prim} using the aproppiate weigthting factors, as explained above. Then, the parameters defined in the *RTPlan,* such as, energy, field size, beam angle or number of monitor units (MU), are used as input data for the *Secondary radiation tool,* which calculates H_{sec}. This tool can be an analytical model, an artificial intelligence (AI) model, or a Monte Carlo simulation. If the plan is a photon plan, H_{sec} represents the photon dose from the 5 % isodose, complementing the contribution from the scatter in the patient and the leakage from the linac head. In addition, in the case of high energy photons (> 8 MV), secondary neutrons should be included. A recent review presented the current possibilities of analytical models [25]. If the plan is a proton plan, H_{sec} represents the secondary neutron and photon field produced during the treatment.

The contribution from imaging, H_{imag}, is obtained by an *Imaging tool*, which similarly to the tool for secondary radiation, can be an analytical model, an AI model or a Monte Carlo simulation. Imaging parameters, such as voltage, exposure, collimator or $CTDI_{vol}$ are extracted from the DICOM files of each scan. The tool could also use the *wbCT*. Since the dose contribution from planar imaging lies in the very low dose range [14], comparable to the calculation uncertainty of the CT and CBCT doses, H_{imag} could include only these two contributions.

An additional input for the tools is a whole-body model of the patient. However, only the *pCT* is usually available for RT patients, covering a portion of the whole body and potentially omitting relevant radiosensitive organs depending on the target's position. Therefore, a reconstruction of the whole-body patient is necessary. This reconstruction is made using an improved version of the Interactive Software for Image Segmentation and Registration (IS^2aR) [26]. This software registers the *pCT* with the ICRP-110 phantom [27] to obtain a transformation matrix, which is later applied to the ICRP phantom. This synthetic patient-specific whole-body CT is representative of the size of our patient. Then, to enhance patient-specificity, a further step involves replacing the original CT scan in the corresponding region within the synthetic phantom. This way, the final synthetic whole-body CT (*wbCT*) reflects the actual geometry of the patient in the area around the target (the sequence of steps can be found in Supplementary Fig. S1). In addition, the segmentation of structures is always required for total organ dose computation. IS^2aR fuses the *RTStruct* with the appropriately modified structures defined in the ICRP-110. If additional structures in the *pCT* are of interest, an automatic segmentator could be used to obtain them (referred to as extra-structures – *Xstruct*).

The three components H_{prim}, H_{sec} and H_{imag} are finally summed. The methodology presented was applied to two lymphoma treatments, one planned with photons and the other with protons. These cases are described in detail in section 2.3.

2.2. Integrating imaging doses to RT doses

Ideally, total dose should be calculated voxel-wise since dose distributions in the organ holds more significance than an organ dose average and are necessary for plan approval and radiobiological calculations, such as NTCP [28,29]. For RISM risk assessment, when the organ is exposed to doses higher than 2 Sv [30], several models are also based on dose distributions or are applied voxel by voxel [31–34]. For organs receiving doses lower than 2 Sv, linear no-threshold models, such as the BEIR [7] or ICRP models [21], can be applied, requiring only the mean dose, so the summation of mean doses could be feasible for these cases.

In the case of the *Imaging tool* several methods which can be found in the literature have in common that they only provide the equivalent dose in organ [35–39]. Thus, to simplify the application of the methodology, given the common features of imaging exposure, in this work we propose a simple approximation for using the mean dose to represent the dose distribution. For this approximation, we performed a comparison between $(H_{prim} + H_{sec})$ and H_{imag} in terms of the dose volume histogram (DVH). DVHs were generated using the same histogram binning as done by the TPS, that is, using the dose binning which covers a range

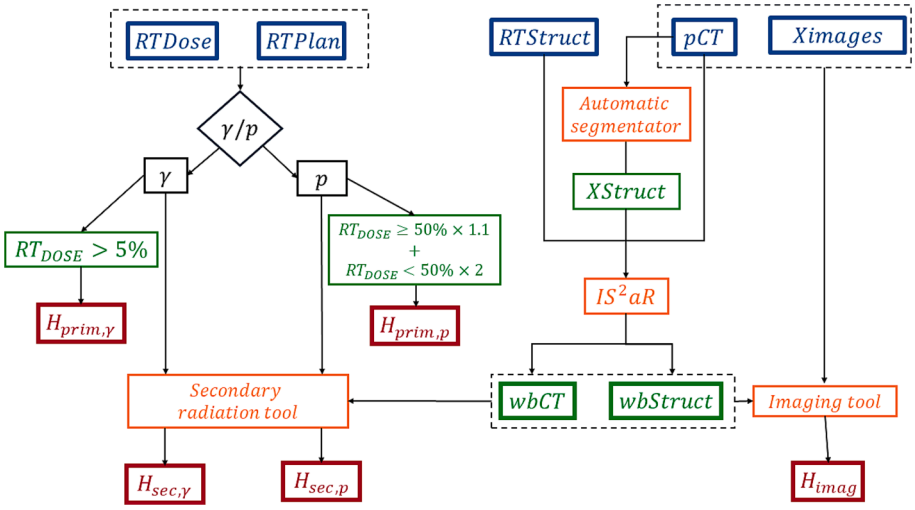

Fig. 1. Flow chart of the proposed total dose calculation methodology. DICOM data from the treatment planning system is used as input: *i) RTDose*, *ii) RTPlan*, *iii) RTStruct*, *iv)* planning CT (*pCT*), and *v)* the additional verification/setup CT and/or CBCT (*Ximages*). The type of plan, photon (γ) or proton (p), determines how to process the RTDose to obtain H_{prim} . Four tools are used for the rest of calculations: *i) Automatic segmentator*, to obtain additional segmentations in the pCT, *ii)* IS^2 *aR*, to create the whole-body CT model of the patient (*wbCT*) with the whole-body segementations (*wbStruct*), *iii) Secondary radiation tool*, to calculate the peripheral photon doses for photon plans ($H_{sec,\gamma}$) or the secondary neutron and photons doses for proton plans ($H_{sec,p}$), and) *iv) Imaging tool*, to calculate the doses from the imaging procedures (H_{imag}), both CT and/or CBCT.

of doses from zero to the maximum dose in the target.

A pelvis treatment was selected for this comparison with all doses experimentally determined using the same dosimetry system, to avoid methodology dependence in the results. Both CT and CBCT were evaluated. In addition, the lymphoma photon case was also used to confirm the results.

2.3. Radiotherapy plans and imaging protocols

2.3.1. Diffuse large B-cell lymphoma (DLBCL) VMAT plan

The DLBCL case consisted of a mediastinal target extending from the jugulum to the top of the heart (see Supplementary Fig. S2a). The plan was calculated using ECLIPSE v. 15.6 (Varian Medical Systems, Inc.) and administered using a TrueBeam Varian linac (Varian Medical Systems, Inc.) with one arc at 6 MV, following the protocol of *Vigo University Hospital Complex* (Spain). The prescription dose to the PTV was 47 Gy in 22 fractions. The imaging protocol of the DLBCL plan also involved a CBCT per fraction and a planning CT. For this patient, the Elekta XVI kV-CBCT system was used with a thorax protocol characterized by a voltage of 120 kVp, a mean exposure of 264 mAs, a kV collimator M20, and the bowtie filter F1. The planning CT was acquired with a Philips Brilliance Big Bore scanner, using the following protocol: 120 kV of voltage, mean exposure of 187 mAs, pitch of 0.813, $CTDI_{vol}$ of 10.99 mGy, beam collimation of 24 mm, and a bowtie filter.

The *pCT* covered the base of the skull to the upper part of the abdomen (see Supplementary Fig. S2a), encompassing sufficient radiosensitive organs for the purpose of this work. Segmentations of the target volume, oesophagus, heart, lungs, and breasts from the TPS were used, while Total segmentator [40] was used to obtain the *XStruct* file containing segmentations for stomach, liver, spleen, and pancreas.

The Periphocal 3D (P3D) software [41] was the selected tool for H_{sec}. P3D is a MATLAB (MathWorks, Inc)-based software that calculates the photon dose distribution on a voxelized input anatomy from some plan parameters: prescribed dose, monitor units, field size, and location of the isocenter. The CBCT doses were obtained by MC simulation using the Elekta's Synergy XVI model implemented with the GATE code (v. 9.2) [42]. The geometries of the system, the beam tube anode, the bowtie filter, and the different existing collimators were considered, as well as the energy spectrum of the anode (120 kV in this case). In the simulation, 10^9 particles were run for each rotation of the phantom to obtain the dose distribution map. Virtual Dose™CT [38] software computed the doses from the *pCT*. This software relies on a comprehensive database of organ doses derived from MC simulations, involving a library of 25 anatomically realistic phantoms. The organ mean doses were calculated from *i)* the CT protocol parameters (mAs, kV, $CTDI_{vol}$, pitch, beam collimation) and *ii)* the scanned volume defined over a patient-representative phantom. The CT dose in the target was evaluated as an average of the dose in the surrounding organs.

MATLAB was used for the summation of the doses coming from the different sources.

2.3.2. Classical Hodgkin lymphoma (cHL) proton plan

The cHL proton plan consisted of a target located in the left supraclavicular fossa, including paratracheal nodes (see Supplementary Fig. S2b). It was designed with the pencil beam scanning (PBS) proton beam of *Skandion Clinic* (Sweden), a Proteus 235 from IBA (Ion Beam Applications, Louvain-La-Neuve, Belgium). The plan calculated using ECLIPSE v.16.1 consisted of two beam incidences at 0° and 10°, with proton energy ranging from 67 to 119 MeV. The prescription was of 20 Gy (RBE) to the Clinical Target Volume (CTV) in 10 fractions. The imaging protocol consisted of one planning and two verification CT scans, as previously mentioned planar images were not considered. The planning CT was acquired with a Philips Brilliance Big Bore scanner, using the following protocol consisting of 120 kV voltage, 192 mAs mean exposure, 0.8 pitch and 11.40 mGy $CTDI_{vol}$, 24 mm of beam collimation, and a bowtie filter. The two verification scans were acquired with a Siemens Definition AS + using 120 kVp, mean exposure 73 mAs and 69 mAs, 0.6 pitch and $CTDI_{vol}$ of 10.17 mGy and 9.56 mGy, beam collimation 38 mm, and a bowtie filter. Daily planar imaging was not considered as explained in Section 2.1.

For this case, the *pCT* only covered the top of the head to the upper part of the thorax, leaving most organs in the abdomen outside the CT scan (see Supplementary Fig. S2b). Therefore, the *wbCT* and *wbStruct* were obtained with IS^2aR. The target volume, thyroid gland and oesophagus segmentations from the *RTStruct* file were used. Total Segmentator was also used to obtain the *XStruct*, containing brain and the portion of lungs included in the CT. The rest of the organs of interest were defined in the IS^2aR phantom: rest of lungs, heart, stomach, liver, spleen, pancreas, gall bladder, kidneys, intestine, urinary bladder, and prostate.

H_{sec} was obtained by a full MC simulation conducted using the previously validated MC model of the proton beam at *Skandion Clinic* [43,44]. The simulation consisted of modelling, energy layer by energy layer, the actual proton spots from the clinical plan. The MCNP 6.2 code was used for the calculations, employing a combination of cross-sections and the Cascade-Exciton Model (CEM) nuclear model for the high-energy range [45]. Proton and photon absorbed doses, and neutron dose equivalent were scored in each voxel of the wbCT. The MC proton dose validated the simulation of the plan in the patient. H_{imag} was calculated with Virtual Dose™CT and MATLAB was used for the summation of all the doses.

2.3.3. Prostate treatment

The pelvis case was a VMAT prostate plan with the addition of a CBCT for each fraction to the planning CT, following the protocol of *Clínica Alemana de Santiago* (Chile). The prescribed dose to the Planning Target Volume (PTV) was 75.6 Gy to the 95 % isodose in 42 fractions (Supplementary Fig. S2c). The VMAT plan, calculated using MONACO v.5.11 (Elekta Solutions AB), comprised one arc at 6 MV delivered by an Elekta Synergy linac (Elekta Solutions AB), with Elekta XVI kV-CBCT system integrated. The protocol for a pelvis CBCT uses 120 kVp, a mean exposure of 1056 mAs, a kV collimator M20, and a bowtie filter F1. A pelvis protocol for the prostate planning CT was applied using a Siemens Somatom Definition AS + scanner (100 kV voltage, 272 mAs mean exposure, 0.8 pitch, and 10.69 mGy CTDIvol).

The VMAT plan was designed for the CIRS anthropomorphic adult phantom (https://www.cirsinc.com/products/radiation-therapy/atom-phantom-family/) with specific holders for thermoluminescent dosimetry (TLD) chips distributed within 22 radiosensitive internal organs. 217 TLDs dosimeters were placed within the 39 slices of the phantom to measure the dose received in one RT fraction, one CBCT fraction, and the planning CT. The equivalent dose in an organ was then evaluated as an average over the dose equivalent measured in the set of positions defining the organ. Using the dose in these positions pseudo-dose volume histograms (as actual dose distribution is not possible) were obtained.

TLD-100 chips of 3.2 × 3.2 × 0.89 mm (ThermonEberline LLC, Oakwood Village, OH 44146 USA) were used for the measurements. An individual sensitivity factor uniquely identifies each TLD chip. The standard deviation (SD) of the response within the group was 5 %. Glow curves were obtained using a Harshaw 3500 reader with the WinREMS operational software (2009, Thermo Eberline). TLDs were processed before and after irradiation following the protocol of Sáez-Vergara [46]. Dose calibration factors were determined for a 6 MV beam and two X-ray beams of 50 kVp and 120 kVp, which were characterized by their HVL values. Those factors allowed us to validate the normalized energy response curve proposed by Duggan *et al.* [47] as a function of the effective energy. Thus, a dose calibration factor for each TLD was calculated from the calibration factor at 6 MV and the corresponding correction due to the effective energy. For the X-ray exposures, effective energies were estimated from the HVLs profiles measured (Radcal Accu Gold model Digitalizer-AGMS-D+) along the CBCT for the prostate

protocol. For the peripheral dose estimation during the prostate cancer treatment delivery with the 6 MV beam, the mean energy curve from Sánchez-Nieto *et al.* [24] was used. For the CT doses, specific calibration factors were determined from the dose measured by the Accu-Gold + Touch Pro with IC 10X6-0.6CT inside the CT phantom and the readings of four TLDs placed at the same point using a homemade suitable holder.

2.4. Plan evaluation

Plan evaluation was conducted using the total dose distribution and, in addition, using the distribution provided by the TPS, as done in the clinic. Dose homogeneity in the target area and dose/volume constraints to the surrounding OARs (see later in Section 3.5) were evaluated. Risk assessment was conducted in terms of lifetime attributable risk (*LAR*) using two different risk models depending on the equivalent dose in an organ. While the Schneider model [31,32] was used for equivalent doses higher than 2 Sv, the linear no-threshold model from BEIR-VII [7] was used for lower doses. *LAR* was evaluated for the age at exposure of each patient, a maximum age of 100 years, and a latency period of 5 years.

The evaluation and comparison were performed only for the lymphoma cases, for which we have complete dose distributions, and for the organs for which risk model parameters can be found in the literature.

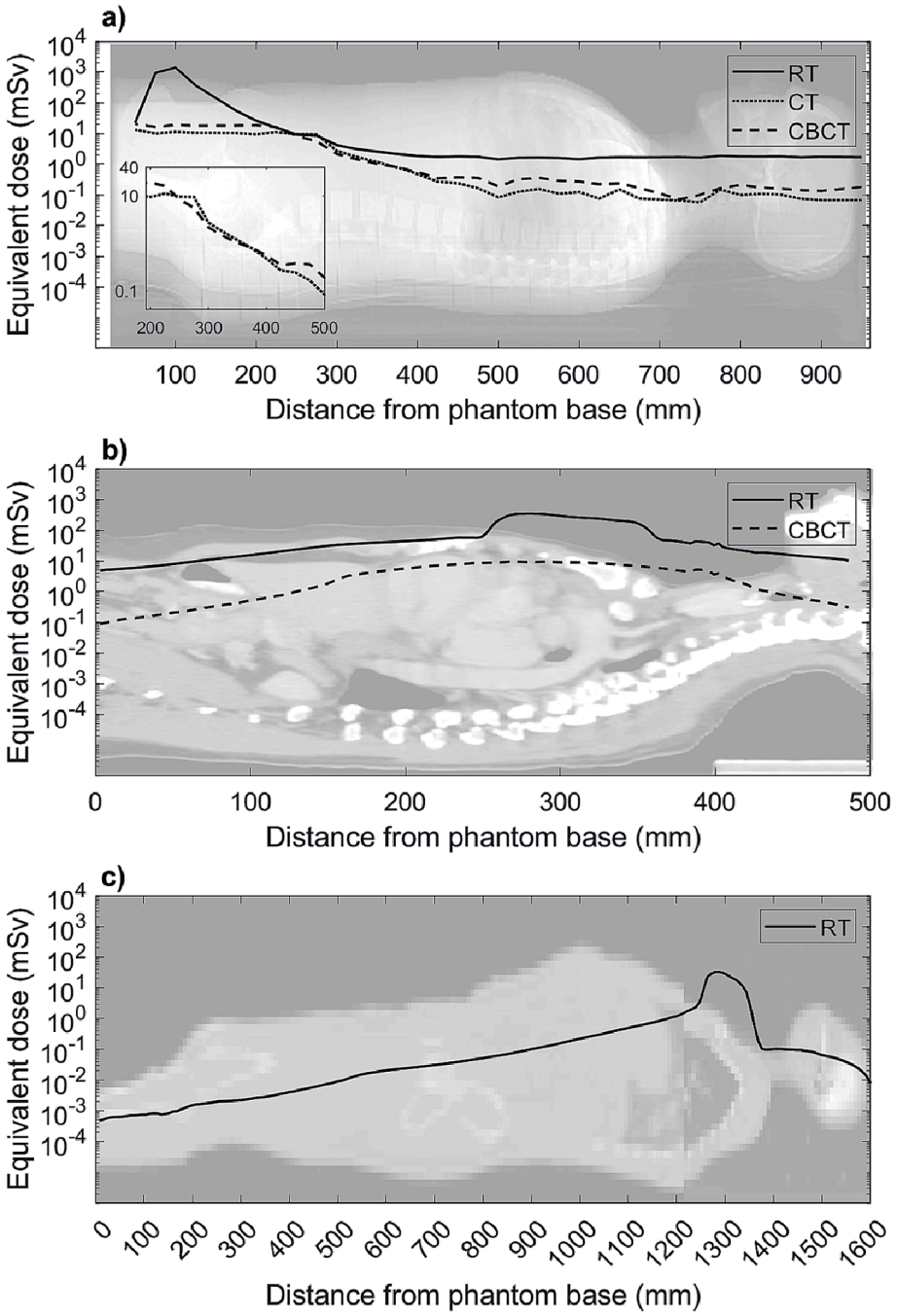

Fig. 2. Mean equivalent dose per slice for a) the prostate VMAT case, b) the diffuse large B-cell lymphoma VMAT case, and c) the classical Hodgkin lymphoma proton PBS case. A sagittal view of each phantom is included for reference and each slice is defined by the distance to the base of the phantom. Insert in a) shows the higher scanned area in CT in comparison to CBCT. Notice that only c) represents the whole body of the patient.

3. Results

3.1. Prostate VMAT case

Fig. 2a shows the mean equivalent dose per slice (defined by the distance to the base of the phantom) measured during one RT fraction, one CBCT fraction, and the planning CT. Results from RT measurements show a gradient from the in-field area with doses in the range of Sv to the peripheral area with doses of the order of a few mSv. The imaging doses from the CBCT and CT show a comparable pattern: two plateau regions separated by a transition region. The first plateau is within the scanned volume, with an average dose of 10.5 (9.36–13.14) mSv for CT and 18.1 (16.01–20.4) mSv for CBCT. The second plateau is beyond the scanned volume with an average dose of 0.103 (0.0568–0.1634) mSv and 0.212 (0.072–0.372) mSv for CT and CBCT, respectively. On average, for this phantom and the imaging protocols, CBCT delivers 1.5 times the CT dose in one fraction, but the scanned volume by CBCT is smaller (see insert in Fig. 2a).

The total equivalent dose in an organ for the 42 treatment fractions ranged from 68 mSv in the oesophagus to 78 Sv in the prostate (see all values in Table 1). The percentual contribution of the different components to the total dose is depicted in Fig. 3a. Except for the testes (which are at the surface and thus have higher dose when irradiated with kV energies), the contribution of imaging doses is lower than RT doses, with a maximum contribution of 28 % (39 of 140 mSv) to the total equivalent dose in the gall bladder and kidneys due to the 42 (one per fraction) CBCTs. The contribution of planning CT is lower than 1 %.

3.2. Diffuse large B-cell lymphoma (DLBCL) VMAT case

Fig. 4a and b show the RT and CBCT dose distributions for one fraction at the isocenter plane. The RT distribution exhibits a steep gradient from the PTV to the rest of the patient (see also Fig. 2b), with doses in the range 0.1–0.2 Sv in the peripheral area. In the distribution of CBCT, the scanned area is well visualized with a more homogeneous distribution with doses of the same range that on the peripheral area from RT (see Fig. 2b). The comparison between Fig. 2a and 2b shows that for this case, the phantom covers up part of the transition area, with doses reduced to the range of 2–4 mSv.

Only those organs entirely inside the CT scan were considered for reporting equivalent dose (see organs in Fig. 3b and Table 2) to maintain consistency with the equivalent doses calculated for the CT, given that Virtual Dose™CT calculates over a whole-body phantom and, thus, over the complete organ volume. This is the reason for not including a curve for CT in Fig. 2b, as the whole distribution in the phantom is not available. When adding all the contributed dose, total organ doses ranged from 1.5 Sv in the pancreas to 48 Sv in the PTV (see all values in Table 2). The contribution of the different components to the total dose is depicted in Fig. 3b. In this case, the contribution of imaging doses is also lower than that of RT doses, with a maximum contribution of 10 % to the heart from CBCT. For the imaging protocols considered, CBCT and CT doses were similar (average factor ~ 1.1) in the organs inside the scanned region defined by the CBCT (oesophagus, heart, lungs and breasts), assuming one fraction. For the rest of the volume, CT doses were on average 4.6 higher than CBCT doses. However, as CBCT is repeated in each fraction of the plan, higher total doses resulted from the CBCT.

Table 1
Equivalent dose in organ measured for the prostate case.

Organs	*H* (mSv)						
	One fraction			Whole treatment (42 fractions)			
	RT	CBCT	CT	RT	CBCT	CT	**Total dose**
Brain	1.7	0.14	8.0×10^{-2}	70	5.8	8.0×10^{-2}	**76**
Thyroid	1.7	0.11	7.0×10^{-2}	72	4.7	7.0×10^{-2}	**77**
Oesophagus	1.4	0.23	9.6×10^{-2}	59	9.6	9.6×10^{-2}	**68**
Heart	1.5	0.34	0.18	63	14	0.18	**78**
Lungs	1.6	0.29	0.11	68	12	0.11	**80**
Stomach	2.3	0.80	0.84	97	33	0.84	$\mathbf{1.3 \times 10^2}$
Liver	1.8	0.48	0.36	77	20	0.36	**98**
Spleen	1.7	0.39	0.30	73	16	0.30	**89**
Pancreas	2.0	0.64	0.69	83	27	0.69	$\mathbf{1.1 \times 10^2}$
Gall bladder	2.4	0.93	0.96	1.0×10^2	39	0.96	$\mathbf{1.4 \times 10^2}$
Kidneys	2.3	0.92	1.0	98	39	1.0	$\mathbf{1.4 \times 10^2}$
Intestine	1.2×10^2	11	9.1	5.1×10^3	4.5×10^2	9.1	$\mathbf{5.6 \times 10^3}$
Urinary bladder	4.8×10^2	20	11	2.0×10^4	8.6×10^2	11	$\mathbf{2.1 \times 10^4}$
Testes	20	26	17	8.5×10^2	1.1×10^3	17	$\mathbf{2.0 \times 10^3}$
Prostate (Target)	1.8×10^3	19	11	7.7×10^4	7.9×10^2	11	$\mathbf{7.8 \times 10^4}$

3.3. Classical Hodgkin lymphoma (cHL) proton PBS case

Fig. 4c illustrates the total dose distribution in the whole body, including protons and neutrons, while the photon contribution was negligible. In Fig. 2c, the mean dose per slice has been plotted. The asymmetry of the plot is due to the difference in volume above (neck and head) and below (thorax and abdomen) the target in the cranio-caudal direction. In comparison with the photon plans, as depicted in Fig. 2a and b, there is a much sharper dose gradient as one moves farther from the target. In photon plans there is a plateau region in the body's periphery due to the linac leakage, which is not shown in the proton treatments. In accordance with the DLBCL case, CT dose distribution in the whole phantom was unavailable and, therefore, not included in Fig. 2c.

Total equivalent dose in an organ ranged from 1.7 mSv in the prostate to 19 Sv in the target (see all values in Table 3). Organs within the treatment field (thyroid, oesophagus, and lungs) received a dose from the total RT treatment of the order of Sv or cSv. The use of the $w_R = 2$ instead of RBE = 1.1 in the out-of-field volume led to an increase in equivalent dose of 1.3 and 1.1 Sv for thyroid and oesophagus, respectively, and 100 mSv for lungs. The CT contribution is very low for these organs, as found for the photon treatments. However, for the rest of organs, RT and CT dose are in the same range, reflected in the higher contribution to the total dose (see Fig. 3c). In fact, for the brain, the imaging dose was higher than the RT dose.

3.4. Integrating imaging doses to RT doses

The left panel of Fig. 5 shows the pDVHs for each exposure in the prostate case for an organ within the different regions described in Section 3.1: the urinary bladder within the scanned volume, the liver in the transition region, and the brain outside the scanned region. When using the same histogram binning as in the RT case, the imaging pDVHs concentrate in the low range of each scale. From the point of view of RT itself, the effect of imaging is equivalent to exposing the whole organ to the same dose. However, we are limited to the dose at a few points of each organ.

Proper DVHs were obtained for the DLBCL case. The first and second columns in the right panel of Fig. 5 show the DVHs of the heart (inside the scanned area) and liver (in the transition area) for the RT and CBCT

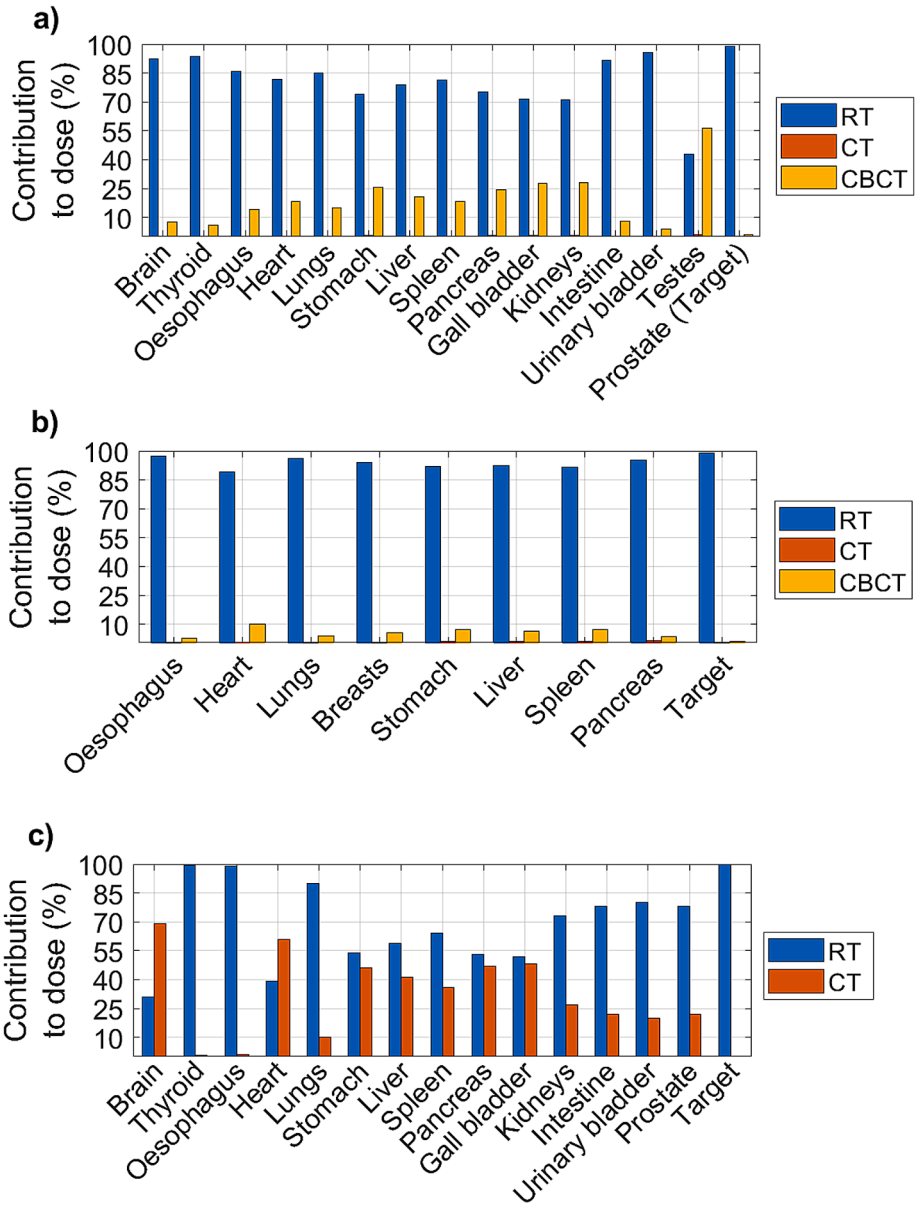

Fig. 3. Contribution of RT and imaging to the total dose received by the patient in the a) the prostate VMAT case, b) the diffuse large B-cell lymphoma VMAT case, and c) the classical Hodgkin lymphoma proton PBS case.

exposures using a binning range defined by the minimum and maximum dose of the organ in the RT exposure. The distribution of the CBCT dose was concentrated within a small interval in comparison to the DVH from RT. The third column shows the DVH when the binning is adjusted to the representative binning of the target (from 0 to 2.4 Sv). Now, more than 81 % of the voxels are allocated in a single bin. Similar results were found for the other organs. This result means that the approximation of a homogeneous dose is valid for the CBCT, and given that, as shown in Fig. 2a, CT and CBCT's behavior was similar, the homogeneous approximation can be extended to CT doses. As a result, for building DVHs, we can assume the same mean dose value for each voxel of the organ. This approach was used for the DLBCL and the cHL treatments by adding the CT doses to obtain the total dose distributions in each organ.

3.5. Plan evaluation using TPS data and total dose

Figs. 6 and 7 display cumulative DVHs for the DLBCL and the cHL plans for OARs included in the planning CT and used for the plan evaluation. The plots depict the curve obtained by the TPS, the curve incorporating out-of-field doses not considered by the TPS (denoted as RT plan in the plot), and the curve corresponding to the total dose, including the imaging doses. The general trend is a shift towards higher doses, as we increase the dose sources. In the photon plan, aside from the target, when adding the peripheral dose, there is a significant shift to the right in the dose range below 5 Sv. From that point onward, TPS and RT curves overlap. The effect of imaging doses is reflected in a globally low shift of the whole curve. For the proton plan, minimal shifts are observed. For the target, RT and total curves overlap, reflecting the low contribution of imaging and a higher contribution from neutrons. The thyroid and the oesophagus exhibit almost indistinguishable curves, as the contribution of neutrons decreases moving farther from the target. In the case of lungs, with a high portion of their volume away from the target and consequently very low doses from the protons, more significant differences between the three are observed for doses lower than 0.4 Sv. The effect is not as pronounced as in the photon plan due to the lower neutron contribution than peripheral photons and the repetition of the CBCT scan in each treatment fraction, which increases the overall imaging dose.

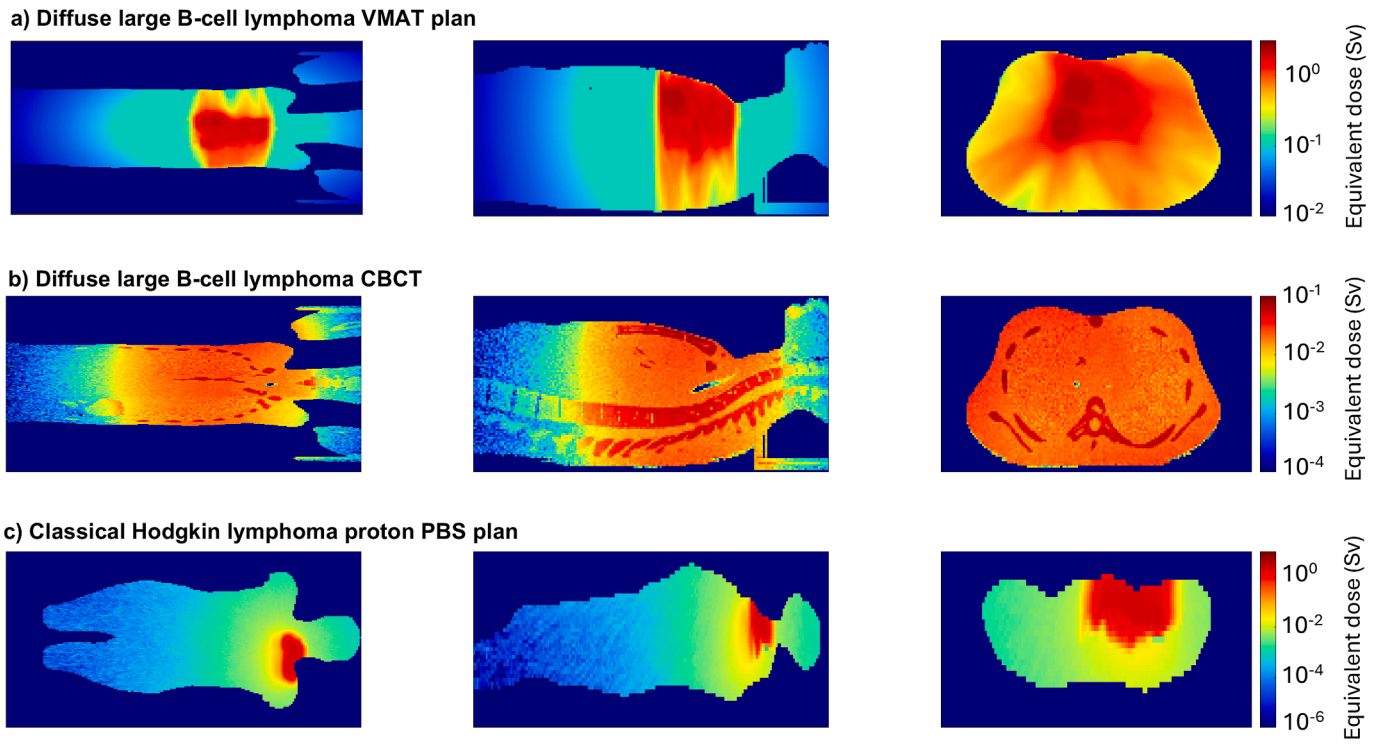

Fig. 4. Dose distribution in the diffuse large B-cell lymphoma (DLBCL) a) VMAT fraction, b) DLBCL CBCT fraction, and c) classical Hodgkin lymphoma proton PBS fraction (c). From left to right: coronal, sagittal and axial views at the isocenter plains.

Table 2
Equivalent dose in organ obtained for the diffuse large B-cell lymphoma VMAT case.

Organs	*H* (mSv)						
	One fraction			Whole treatment (22 fractions)			
	RT	CBCT	CT	RT	CBCT	CT	**Total dose**
Oesophagus	7.8×10^2	21	18	1.7×10^4	4.5×10^2	18	$\mathbf{1.8 \times 10^4}$
Heart	1.5×10^2	17	19	3.2×10^3	3.7×10^2	19	$\mathbf{3.6 \times 10^3}$
Lungs	5.1×10^2	20	20	1.1×10^4	4.3×10^2	20	$\mathbf{1.2 \times 10^4}$
Breasts	3.8×10^2	23	17	8.4×10^3	5.0×10^2	17	$\mathbf{9.0 \times 10^3}$
Stomach	8.1×10^2	6.4	18	1.8×10^3	1.4×10^2	18	$\mathbf{1.9 \times 10^3}$
Liver	9.3×10^2	6.5	21	2.1×10^3	1.4×10^2	21	$\mathbf{2.2 \times 10^3}$
Spleen	9.3×10^2	7.3	23	2.0×10^3	1.6×10^2	23	$\mathbf{2.2 \times 10^3}$
Pancreas	65	2.4	21	1.4×10^3	52	21	$\mathbf{1.5 \times 10^3}$
Target	2.2×10^3	20	19	4.8×10^4	4.3×10^2	19	$\mathbf{4.8 \times 10^4}$

From a planning perspective, the differences in the curves do not have clinical relevance, as reflected by the minimal changes in the objectives and constraints considered during planning tabulated in Table 4. The only exception is the $V_{2.5\ Gy\ (RBE)}$ for breast in the photon plan, where the percentage of volume receiving at least 2.5 Sv increased from 55 to almost 100 %.

Regarding the effect on risk assessment, Table 5 presents the *LAR* estimated using the Schneider or the BEIR-VII model, according to the level of equivalent dose. For organs where the BEIR model was used, considering the total dose resulted in a significant increase in the value. The increment is infinite in those organs in the proton plan where TPS assigned no dose. However, the absolute value of the risk is lower than 1 %. When the Schneider model was used for organs close to the target, receiving doses of tens of Sv, much higher risks were estimated. The consideration of total dose led to an increase in the predicted risk of around 20 or 30 % for the lungs and the breasts, respectively.

4. Discussion

In this study, we introduced a methodology to integrate in-field, out-of-field, and imaging doses administered to patients throughout their course of RT treatment, covering clinically relevant numbers and protocols of imaging procedures. The analysis of total dose can be conducted retrospectively or prospectively, relying on TPS data for in-field doses to simplify calculations. Experimental results were presented primarily to justify the integration of imaging doses rather than the methodology itself. The main limitation of measurements lies in their inherent limitation to evaluate doses at specific positions and their use of generic anthropomorphic phantoms that may not accurately reflect a patient's actual anatomy. As De Saint-Hubert et al. [48] noted, measurements are recommended primarily to validate both the *Secondary radiation* and the *Imaging tools*. Regarding these tools, we prefer the use of analytical or AI models over MC simulations for their convenience in clinical routine. While MC simulations require longer computational times and greater resources, faster options like MOQUI are being introduced [49]. Nevertheless, both types of resources were used in our work. In proton therapy, although we employed MC simulations to evaluate neutron radiation, alternative analytical models are available in the literature [50,51].

For evaluating imaging doses, most automated solutions provide organ mean doses, which need to be integrated with RT dose distributions. Traditional plan evaluation is based on DVHs, which cover a dose range from zero to the maximum dose in the target. Fig. 5 illustrates that the distribution of organ imaging doses is nearly uniform compared to doses from RT fractions. Our approach aligns with findings from Ding et al. [52], where CBCT dose distribution was evaluated using MC

Table 3
Equivalent dose in organ obtained for the proton HL case.

Organs	H (mSv)										
	One fraction						Whole treatment (10 fractions)				
	RT			CT			RT		CT	**Total dose**	
	Protons		Neutrons	Planning	Verif. 1	Verif. 2					
	$w_R = 2$	$RBE = 1.1$					$w_R = 2$	$RBE = 1.1$		$\boldsymbol{w_R = 2}$	$\boldsymbol{RBE = 1.1}$
Brain	0	0	1.3	8.9	8.5	8.3	13	13	26	**38**	**38**
Thyroid	6.5×10^2	5.2×10^2	8.9	12	11	11	6.6×10^3	5.3×10^3	33	$\mathbf{6.6 \times 10^3}$	$\mathbf{5.3 \times 10^3}$
Oesophagus	5.2×10^2	4.1×10^2	15	15	14	13	5.4×10^3	4.2×10^3	42	$\mathbf{5.4 \times 10^3}$	$\mathbf{4.2 \times 10^3}$
Heart	0	0	3.9	26	18	15	39	39	59	**98**	**98**
Lungs	39	29	10	23	17	15	4.9×10^2	3.9×10^2	55	$\mathbf{4.9 \times 10^2}$	$\mathbf{4.1 \times 10^2}$
Stomach	0	0	1.7	5.0	2.9	2.2	17	17	10	**28**	**28**
Liver	0	0	1.5	3.6	2.2	1.7	15	15	7.5	**22**	**22**
Spleen	0	0	2.0	3.7	2.3	1.9	20	20	7.9	**28**	**28**
Pancreas	0	0	1.2	4.2	2.6	2.1	12	12	8.9	**20**	**20**
Gall bladder	0	0	1.1	3.5	2.1	1.6	11	11	7.3	**18**	**18**
Kidneys	0	0	1.0	1.5	1.0	0.80	9.7	9.7	3.3	**13**	**13**
Intestine	0	0	0.68	0.44	0.30	0.25	6.8	6.8	1.0	**7.8**	**7.8**
Urinary bladder	0	0	0.20	0.18	0.13	0.11	2.0	2.0	0.42	**2.4**	**2.4**
Prostate	0	0	0.14	0.14	0.10	8.0×10^{-2}	1.4	1.4	0.32	**1.7**	**1.7**
Target	1.8×10^3	1.8×10^3	25	12	11	11	1.9×10^4	1.9×10^4	33	$\mathbf{1.9 \times 10^4}$	$\mathbf{1.9 \times 10^4}$

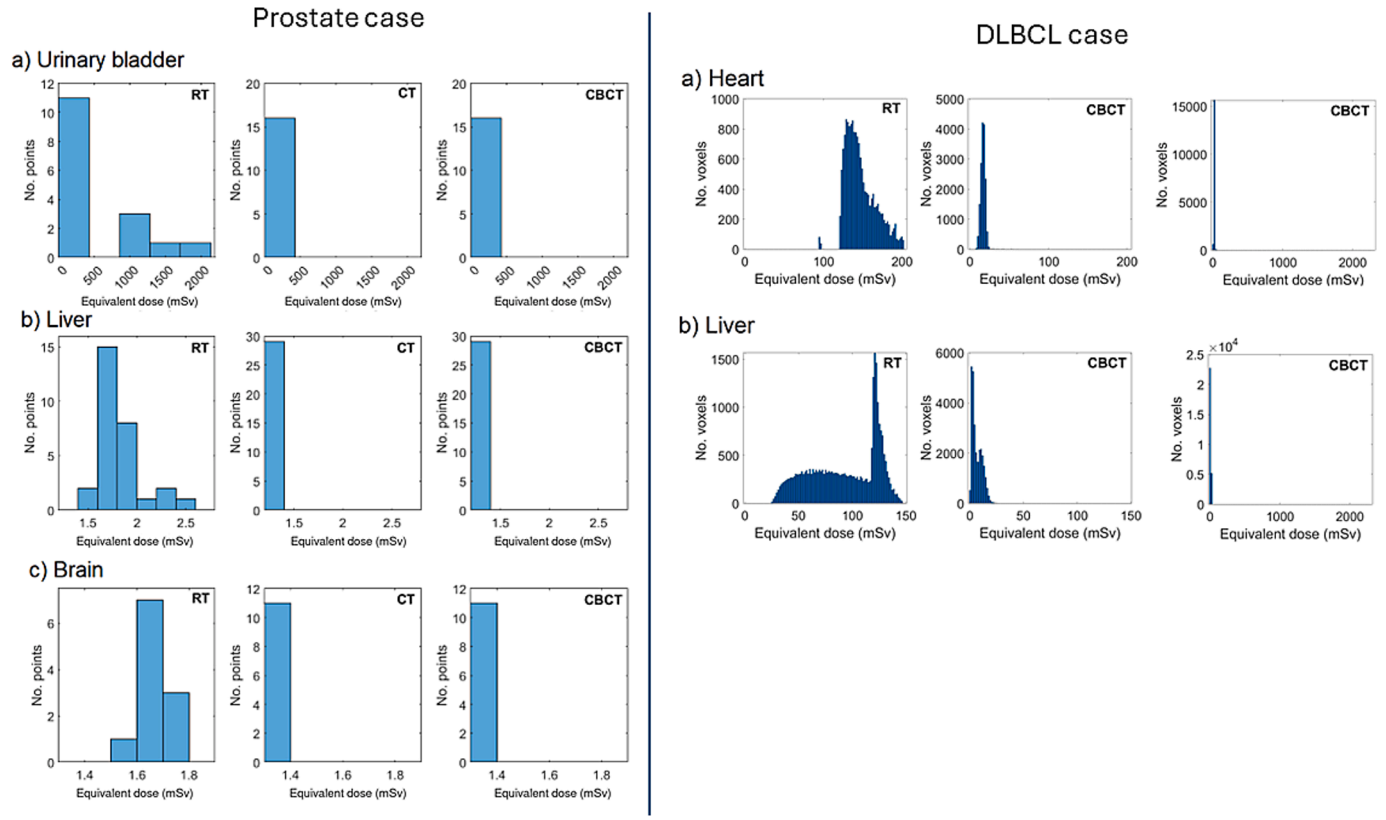

Fig. 5. Left panel: Pseudo-dose volume histograms (pDVHs) in the prostate case for the a) urinary bladder, b) liver and c) brain. pDVHs were built using the binning adjusted between the minimum and maximum dose received by each organ in the RT exposure. Right panel: DVHs in the diffuse large B-cell lymphoma VMAT case for the a) heart and b) liver. DVHs in first and second column were built using the binning adjusted between the minimum and maximum dose received by each organ in the RT exposure, while the representative binning from target was used in the third column.

simulation. Thus, our approximation facilitates straightforward integration of imaging doses into total dose evaluation. Additionally, as suggested in the AAPM TG-180 report, simple approaches that provide reasonable estimates of imaging dose may suffice, given the minimal dose contribution from imaging [19].

In contrast to the limitations of measurements related to patient anatomy, calculations can be performed on the actual patient geometry, providing a detailed dose distribution. However, this is strictly applicable only within the area covered by the pCT. As shown in the DLBCL VMAT case, this image set covered a significant portion of the patient's trunk with involvement of an adequate number of organs. However, for the proton cHL patient, reconstruction of body geometry was necessary. Acquiring a whole-body CT scan was deemed unjustified due to additional dose concerns. Various approaches exist to generate a whole-body model, such as selecting the most appropriate computational phantom from a library or creating a synthetic model of whole-

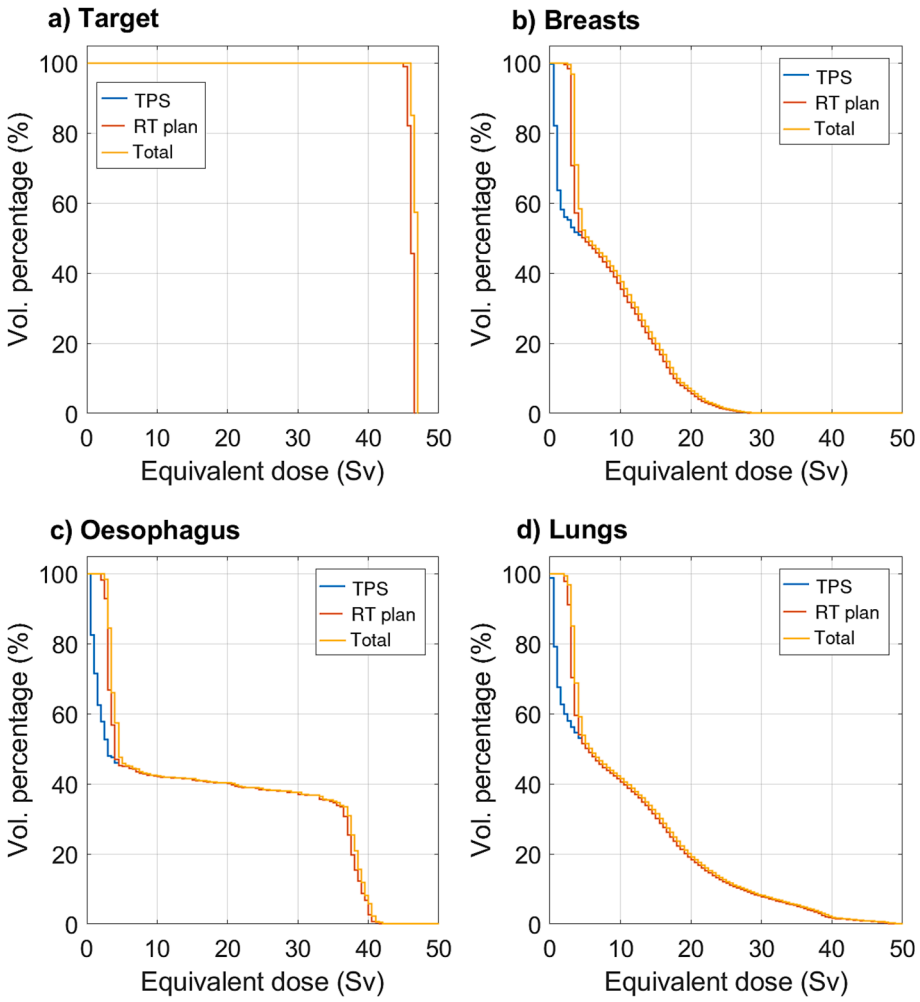

Fig. 6. Cumulative dose volume histograms for the diffuse large B-cell lymphoma VMAT plan for the a) target (PTV), b) breasts, c) oesophagus and d) lungs.

body anatomy [53–56]. Our approach using IS^{2}aR, which combines the patient's real CT and a size-adjusted whole-body phantom, was estimated to offer the best individualized geometry.

The values obtained for the three treatments for the RT and imaging doses are consistent with those elsewhere. Regarding RT doses, the doses reported are in agreement with Sánchez-Nieto *et al.* 2019 [57] and 2022 [41], Harrison *et al.* [58], and Newhauser et al [59]. Regarding imaging doses, our results are in agreement with Ding et al. [52], Hälg *et al.* [14], Shah *et al.* [60], Hashim *et al.* [61], and Lee *et al.* [62] for both CBCT and CT doses for the different imaging protocols.

Our findings indicate that the contribution of the imaging dose is generally low compared to the dose administered during RT treatment. However, the impact of CT and CBCT varies based on the imaging protocol followed. The prospective cohort study carried out by Smith-Bindmand *et al.* [63] showed that the dose is primarily driven by how CT scanners are used, that is, the technical parameters, and not to factors related to the patient, institution, or machine. Jansen *et al.* [35] concluded that the tube currents and exposure times, combined under the exposure, used in clinical practice mainly determine the patient dose level in CT. Our results show a higher contribution from CBCT due to its use in each RT fraction. These results align with existing literature, although a study on a paediatric brain patient found CT doses more than one order of magnitude higher than CBCT [48]. Therefore, the specific percentual contribution of imaging to each organ should be considered as particular of the imaging protocol, although the general trend is extrapolatable. Thus, the contribution depends on the position of the organ relative to the target. Organs near the target exhibit lower contributions. For example, in the DLBCL VMAT treatment, CBCT and CT represent 3.7 and 0.17 % of the total lung dose, respectively. In the prostate VMAT treatment, CBCT and CT contributions were 4.1 and 0.053 % for the urinary bladder. As the organ is farther from the target, the dose due to the RT treatment decreases more rapidly than the dose due to the imaging procedure, leading to an increased relative contribution of the latter. For instance, in the prostate treatment, dose contribution for the stomach were 26 % and 0.64 % for CBCT and CT, respectively. In the case of proton PBS therapy, the contribution of the CT was significantly higher than in photon therapy (46 % for stomach). However, this case may not be representative of the imaging protocol in proton therapy. In fact, a survey on practice patterns of image guidance techniques in 19 European particle therapy centres showed no consensus on their use [64]. In our facility, for example, the number of verification CTs for cHL patients may vary between 2 and 11, with average numbers around 7. If we consider that our patient was exposed to 11 verification CTs, the contribution of CT to total would be even higher (66 % for stomach). However, this high contribution results from the dose reduction around the target in proton therapy, placing the out-of-field RT dose in the same order of magnitude as the imaging doses. This emphasizes the importance of considering the absolute dose values, as even an apparent high relative contribution may still have a low effect.

Regarding the impact of considering the total dose versus relying only on TPS data for planning, the analysis of the cumulative DVHs according to primary planning objectives/constraints showed slightly higher values, although clinical consequences would be expected to be

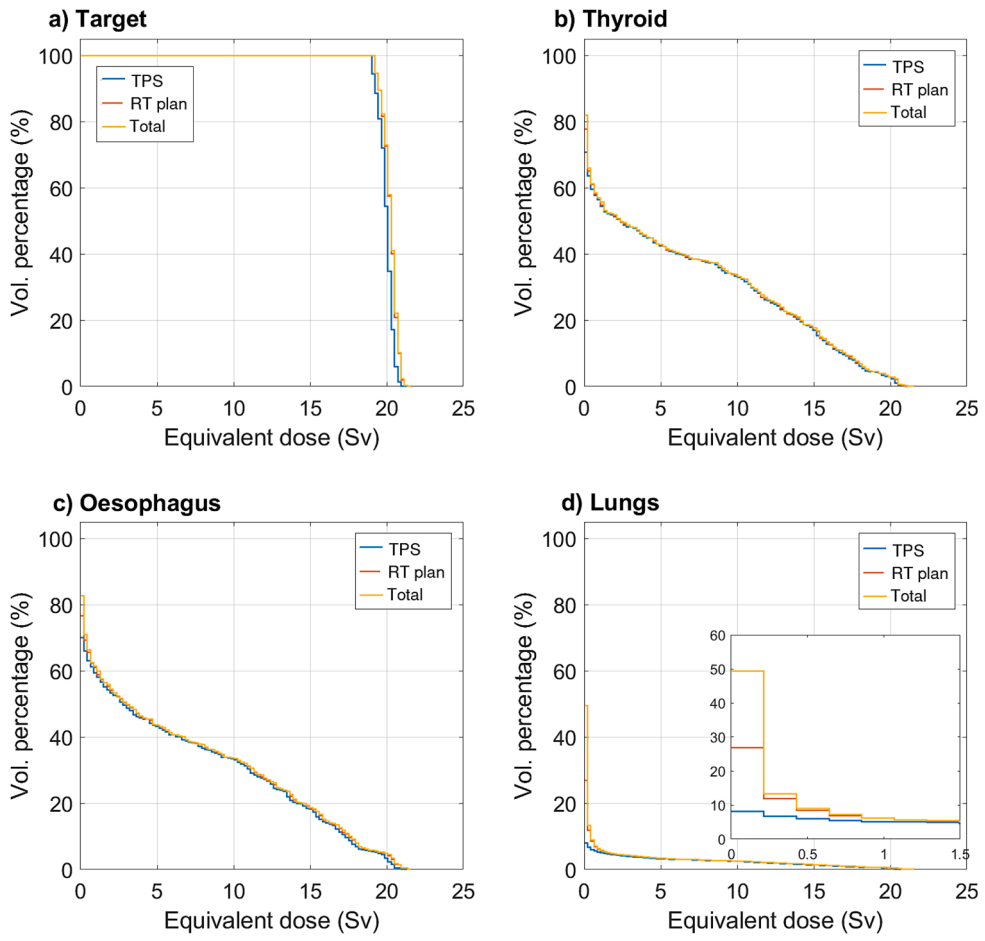

Fig. 7. Cumulative dose volume histograms for the classical Hodgkin lymphoma proton PBS plan for the a) target (CTV), b) thyroid, c) oesophagus and d) lungs.

minimal. However, there is scope for discussion regarding the implementation of image guidance techniques. As the introduction outlines, AAPM TG-180 recommends incorporating imaging dose into treatment planning if it's expected to exceed 5 % of the prescribed target dose [19]. In the cases examined in this study, this threshold was not met in the target: 1 % for the prostate VMAT, 0.9 % for the DLBCL VMAT and 0.2 % for the cHL proton PBS. Nevertheless, when compared to the dose received in a single RT fraction, all CBCT scans accounted for nearly half (44 %) of the dose for the prostate case, and 20 % for the DLBCL case. A similar analysis of OARs leads to different conclusions. For instance, in the prostate case, the urinary bladder received 4 % of the dose solely from CBCT, almost equivalent to receiving two extra RT fractions (factor of 1.8). Particularly noteworthy is the case of testes, superficial organs, which received a dose from all CBCT scans 1.3 times higher than the dose from the RT treatment alone, elevating the total dose to up to 2 Sv. Thus, superficial organs merit special consideration for assessing the total dose. Unfortunately, we were unable to report the dose to the thyroid in the DLBCL VMAT case to confirm a similar pattern. Nevertheless, such discussions could shed light on selecting optimal imaging protocols, including reconsidering the number of CBCT images needed. Conversely, a preliminary evaluation of the total dose could predict the impact of including CBCT for cHL patients, a practice not yet implemented in our institution.

Concerning RISM risk assessment, including out-field and imaging doses resulted in higher risks, as could be expected, with relative increases exceeding 20 %. However, as previously noted, the values may still imply lower risks in absolute terms. For instance, RISM risks using the BEIR model were below 1 % for the considered organs, whereas with the Schneider model, risks ranged from 12 % to 17 %. These differences may not be deemed significant given the uncertainties in risk models. In addition, one should consider that frequent use of image guidance for setup verification or verification of anatomy has allowed the decrease of the margins around the CTV for both proton and photon therapy, implicitly decreasing the doses to the OARs close to the target, this being one of the justifications of IGRT. Nonetheless, reporting the total dose could enhance the value of epidemiological registries, thereby refining the development or adjustment of risk models.

In this study, we evaluated the biologically equivalent proton dose using two different factors to weigh the proton absorbed dose. Our motivation was based on the uncertainties about the use of a constant clinical RBE equal to 1.1, as well as the TG-256 stating that "if one chose an RBE different from 1.1 as an average value, one should distinguish between tumours and organs at risk, that is, choosing a conservative, higher RBE for normal structures and a conservative lower RBE for tumours" [22]. Given that proton dose distribution is localized around the target, this discussion primarily impacts a few patient organs. Specifically, only the thyroid, esophagus, and lungs were exposed to proton doses in the case under study. The use of the $w_R = 2$ in the out-of-field volume resulted in an increase in equivalent dose of 1.3 and 1.1 Sv for the thyroid and oesophagus, respectively, and 100 mSv for lungs. The range of doses for thyroid and oesophagus are more relevant for deterministic effects. In the case of the lungs, the increased dose raised the calculated LAR from 0.77 to 0.89 %, which is not considered a significant difference due to uncertainties in risk models. Nevertheless, further experiments are necessary to improve the knowledge of proton RBE for well-defined tumour types and critical structures and establish a new consensus [22]. As commercial TPS systems are progressively incorporating the assessment of variable RBE, the dose-modifying factor could

Table 4
Plan objectives/constrains for the thorax plans according to TPS dose and total dose.

Volume	Objective/ constraint	VMAT plan		Proton PBS plan	
		TPS	Total dose	TPS	Total dose
Target	$D_{2\%} \leq 105$ %	98.93 %	100.0 %	103.46 %	104.84 %
	$D_{98\%} > 95$ %	95.85 %	96.99 %	94.36 %	95.44 %
Oesophagus	$D_{2\%}$ as low as possible	85.50 %	86.30 %	100.74 %	102.32 %
	$V_{34Gy} < 50$ %	37.42 %	37.43 %	–	–
Thyroid	$D_{2\%}$ as low as possible	–	–	100.66 %	101.69 %
Lungs	$D_{2\%}$ as low as possible	83.65 %	84.85 %	60.01 %	62.38 %
	$V_{5\ Gy(RBE)} < 55$ %	50.22 %	51.52 %	3.21 %	3.38 %
	$V_{20\ Gy(RBE)} < 30$ %	18.34 %	19.21 %	0.30 %	0.49 %
	$D_{mean} < 10$ Gy (RBE)*	10.34 Sv	11.67 Sv	0.39 Sv	0.55 Sv
Breasts	$V_{2.5Gy(RBE)}$ as low as possible	55.18 %	99.63 %	–	–
	$V_{20Gy(RBE)}$ as low as possible	5.56 %	6.38 %	–	–
	$D_{mean} < 4$ Gy(RBE)	7.41 Sv	8.96 Sv	–	–
	$D_{max} < 20$ Gy	30.4 Sv	30.88 Sv		

*This constraint is not aplicable to the VMAT plan, given the higher prescription, but it was almost achieved.

Table 5
Life-time attributable risk (*LAR*) for particular organs in the thorax plans.

Plan	Organ	Risk model	*LAR*(%)		Ratio
			TPS	Total dose	
Diffuse large B-cell lymphoma VMAT plan	Lungs	Schneider	14	17	1.19
	Breasts	Schneider	12	16	1.29
	Stomach	BEIR	0.073	0.79	10.8
	Liver	BEIR	0.027	0.25	9.17
Classical Hodgkin lymphoma proton PBS plan	Lungs	BEIR	0.51	0.72	1.41
	Stomach	BEIR	0	0.0097	
	Liver	BEIR	0	0.0059	
	Urinary bladder	BEIR	0	0.0023	
	Prostate	BEIR	0	0.00074	

be computed over the CT grid, enabling voxel-wise evaluation of equivalent dose in OARs.

5. Conclusions

A methodology has been developed to integrate in-field, out-of-field, and imaging doses providing a comprehensive assessment of the total dose received throughout the entire RT chain. In the study, various scenarios for obtaining the different doses, encompassing both measurement and calculation approaches, have been presented and analysed. Based on our findings regarding CT and CBCT doses, we have proposed a straightforward approximation involving the evaluation of imaging dose distributions using mean doses, which can be readily obtained from coefficient factors, software applications, or AI models. Furthermore, analytical models for out-out-field doses in both photon and proton RT can complement the in-field doses from the TPS. As a result, the integration of all these models into our methodology enables the consideration of the total dose for several purposes:

i) Optimization: Designing strategies to minimize unnecessary exposures and reduce potential long-term side effects for both the RT plan and the imaging protocols.
ii) Prospective risk predictions: Assessing potential risks associate with the radiation exposure.
iii) Retrospective epidemiological analyses: Enhancing our understanding of the impact of radiation on patient outcomes over time.

An additional advantage of our approach is that the calculations performed within the whole-body patient model ensure individualized results.

Consideration of imaging doses in the assessment underscores the importance of being aware of radiation exposure associated with the imaging modalities increasingly used to guide radiation treatment. It is important to note that image guidance is critical for achieving accurate and precise radiation delivery. From this perspective, the increased dose burden may be regarded as the price to pay for the benefits of advanced radiation therapy modalities like proton therapy. Nevertheless, good radiation protection practices dictate that less dose intensive image guidance may be warranted whenever possible, without jeopardising the accuracy of highly conformal dose distributions to the target. In future epidemiological studies on the incidence of RISM in patient cohorts receiving radiation therapy with modern techniques, the frequency of imaging and the dose of it must be considered. In this context, the results of our studies indicate the need to record total doses.

Declaration of competing interest

The authors declare that they have no known competing financial interests or personal relationships that could have appeared to influence the work reported in this paper.

Acknowledgments

This project has received funding from Euratom's Research and Innovation Programme 2019-20 under grant agreement no. 945196.

Appendix A. Supplementary data

Supplementary data to this article can be found online at https://doi.org/10.1016/j.ejmp.2024.104879.

References

[1] Newhauser WD, de Gonzalez AB, Schulte R, Lee C. A review of radiotherapy-induced late effects research after advanced technology treatments. Front Oncol 2016;6:13. https://doi.org/10.3389/fonc.2016.00013.
[2] The International Commission on Radiation Units and Measurements. Report 83: Prescribing, recording, and reporting photon-beam intensity-modulated radiation therapy (IMRT). Journal of the ICRU 2010;10. doi:10.1093/jicru/ndq002.
[3] Harrison R. Out-of-field doses in radiotherapy: input to epidemiological studies and dose-risk models. Phys Med 2017;42:239–46. https://doi.org/10.1016/j.ejmp.2017.02.001.
[4] Berrington de Gonzalez A, Apostoaei AI, Veiga LHS, Rajaraman P, Thomas BA, Hoffman FO, et al. RadRAT: a radiation risk assessment tool for life-time cancer risk projection. J Radiol Prot 2012;32:205–22. https://doi.org/10.1088/0952-4746/32/3/205.
[5] Trott K. Special radiobiological features of second cancer risk after particle radiotherapy. Phys Med 2017;42:221–7. https://doi.org/10.1016/j.ejmp.2017.05.002.

[6] Xiang M, Chang DT, Pollom EL. Second cancer risk after primary cancer treatment with three-dimensional conformal, intensity-modulated, or proton beam radiation therapy. Cancer 2020;126(15):3560–8. https://doi.org/10.1002/cncr.32938.

[7] National Research Council (NRC). Health Risks from Exposure to Low Levels of Ionizing Radiation: BEIR VII Phase 2. Washington, DC: The National Academies Press; 2006.

[8] Galloway TJ, Indelicato DJ, Amdur RJ, Swanson EL, Smith AA, Marcus RB. Second tumors in pediatric patients treated with radiotherapy to the central nervous system. Am J Clin Oncol 2012;35(3):279–83. https://doi.org/10.1097/COC.0b013e318210f533.

[9] Diallo I, Haddy N, Adjadj E, Samand A, Quiniou E, Chavaudra J, et al. Frequency distribution of second solid cancer locations in relation to the irradiated volume among 115 patients treated for childhood cancer. Int J Radiat Oncol Biol Phys 2009;74:876–83. https://doi.org/10.1016/j.ijrobp.2009.01.040.

[10] Xu X, Bednarz B, Paganetti H. A review of dosimetry studies on external-beam radiation treatment with respect to second cancer induction. Phys Med Biol 2008; 53:R193–241. https://doi.org/10.1088/0031-9155/53/13/R01.

[11] Hägl R, Schneider U. Neutron dose and its measurement in proton therapy-current state of knowledge. Brit J Radiol 2020;93:20190412. https://doi.org/10.1259/bjr.20190412.

[12] Mazonakis M, Damilakis J. Out-of-field organ doses and associated risk of cancer development following radiation therapy with photons. Phys Med 2021;90:73–82. https://doi.org/10.1016/j.ejmp.2021.09.005.

[13] Rühm W, Harrison RM. High CT doses return to the agenda. Radiat Environ Biophys 2020;59(1):3–7. https://doi.org/10.1007/s00411-019-00827-9.

[14] Hälg RA, Besserer J, Schneider U. Systematic measurements of whole-body imaging dose distributions in image-guided radiation therapy. Med Phys 2012;39 (12):7650–61. https://doi.org/10.1118/1.4758065.

[15] Rehani MM, Yang K, Melick ER, Heil J, Šalát D, Sensakovic WF, et al. Patients undergoing recurrent CT scans: assessing the magnitude. Eur Radiol 2020;30(4): 1828–36. https://doi.org/10.1007/s00330-019-06523-y.

[16] Murphy MJ, Balter J, Balter S, BenComo JA, Das IJ, Jiang SB, et al. The management of imaging dose during image-guided radiotherapy: report of the AAPM task group 75. Med Phys 2007;34(10):4041–63. https://doi.org/10.1118/1.2775667.

[17] Little MP, Wakeford R, Bouffler SD, Abalo K, Hauptmann M, Hamadaet N, et al. Review of the risk of cancer following low and moderate doses of sparsely ionising radiation received in early life in groups with individually estimated doses. Environ Int 2022;159:106983. https://doi.org/10.1016/j.envint.2021.106983.

[18] Hauptmann M, Byrnes G, Cardis E, Bernier MO, Blettner M, Dabin J, et al. Brain cancer after radiation exposure from CT examinations of children and young adults: results from the EPI-CT cohort study. Lancet Oncol 2023;24(1):45–53. https://doi.org/10.1016/S1470-2045(22)00655-6.

[19] Ding GX, Alaei P, Curran B, Flynn R, Gossman M, Mackieet TR, et al. Image guidance doses delivered during radiotherapy: quantification, management, and reduction: report of the AAPM therapy physics committee task group 180. Med Phys 2018;45(5):e84–99. https://doi.org/10.1002/mp.12824.

[20] European Union. Council Directive 2013/59/Euratom. Official Journal of the European Union 2014;57. https://eur-lex.europa.eu/legal-content/EN/ALL/?uri=OJ:L:2014:013:TOC.

[21] International Commission on Radiological Protection. The 2007 Recommendations of the International Commission on Radiological Protection. ICRP Publication 103. Ann. ICRP 2007;3(7):2–4.

[22] Paganetti H, Blakely E, Carabe-Fernandez A, Carlson DJ, Das IJ, Dong L, et al. Report of the AAPM TG-256 on the relative biological effectiveness of proton beams in radiation therapy. Med Phys 2019;46(3):e53–78. https://doi.org/10.1002/mp.13390.

[23] Howell RM, Scarboro SB, Kry SF, Yaldo DZ. Accuracy of out-of-field dose calculations by a commercial treatment planning system. Phys Med Biol 2010;55 (23):6999–7008. https://doi.org/10.1088/0031-9155/55/23/S03.

[24] Sánchez-Nieto B, Medina-Ascanio KN, Rodríguez-Mongua JL, Doerner E, Espinoza I. Study of out-of-field dose in photon radiotherapy: a commercial treatment planning system versus measurements and Monte Carlo simulations. Med Phys 2020;47(9):4616–25. https://doi.org/10.1002/mp.14356.

[25] Benzazon N, Colnot J, de Kermenguy F, Achkar S, de Vathaire F, Deutsch E, et al. Analytical models for external photon beam radiotherapy out-of-field dose calculation: a scoping review. Front Oncol 2023;13:1197079. https://doi.org/10.3389/fonc.2023.1197079.

[26] Muñoz-Hernández IS, Espinoza I, López-Martínez IN, Sánchez-Nieto B. IS^{2}aR, a computational tool to transform voxelized reference phantoms into patient-specific whole-body virtual CTs for peripheral dose estimation. Phys Med 2023;116: 103183. https://doi.org/10.1016/j.ejmp.2023.103183.

[27] Ann ICRP 2009;39(2).

[28] Lyman JT. Complication probability as assessed from dose-volume histograms. Radiat Res Suppl 1985;8:S13–9.

[29] Kutcher GJ, Burman C. Calculation of complication probability factors for nonuniform normal tissue irradiation: the effective volume method. Int J Radiat Oncol Biol Phys 1989;16:1623–30. https://doi.org/10.1016/0360-016(89)90972-3.

[30] Kry SF, Bednarz B, Howell RM, Dauer L, Followill D, Klein E, et al. AAPM TG 158: measurement and calculation of doses outside the treated volume from external-beam radiation therapy. Med Phys 2017;44(10):e391–429. https://doi.org/10.1002/mp.12462.

[31] Schneider U, Zwahlen D, Ross D, Kaser-Hotz B. Estimation of radiation-induced cancer from three-dimensional dose distributions: concept of organ equivalent dose. Int J Radiat Oncol Biol Phys 2005;61(5):1510–5. https://doi.org/10.1016/j.ijrobp.2004.12.040.

[32] Schneider U, Sumila M, Robotka J. Site-specific dose-response relationships for cancer induction from the combined Japanese A-bomb and Hodgkin cohorts for doses relevant to radiotherapy. Theor Biol Med Model 2011;8:27. https://doi.org/10.1186/1742-4682-8-27.

[33] Dasu A, Toma-Dasu I, Olofsson J, Karlsson M. The use of risk estimation models for the induction of secondary cancers following radiotherapy. Acta Oncol 2005;44(4): 339–47. https://doi.org/10.1080/02841860510029833.

[34] Timlin C, Loken J, Kruse J, Miller R, Schneider U. Comparing second cancer risk for multiple radiotherapy modalitites in survivors og Hodgkin lymphoma. Br J Radiol 2021;94:20200354. https://doi.org/10.1259/bjr.20200354.

[35] Jansen JT, Shrimpton PC, Edyvean S. CT scanner-specific organ dose coefficients generated by Monte Carlo calculation for the ICRP adult male and female reference computational phantoms. Phys Med Biol 2022;67(22). https://doi.org/10.1088/1361-6560/ac9e3d.

[36] Lee C, Kim KP, Bolch WE, Moroz BE, Folio L. NCICT: a computational solution to estimate organ doses for pediatric and adult patients undergoing CT scans. J Radiol Prot 2015;35:891–909. https://doi.org/10.1088/0952-4746/35/4/891.

[37] Stamm G, Nagel HD. CT-Expo—a novel program for dose evaluation in CT. Rofo 2002;174:1570–6. https://doi.org/10.1055/s-2002-35937.

[38] Ding A, Gao Y, Liu H, Caracappa PF, Long DJ, Bolch WE, et al. Virtual Dose: a software for reporting organ doses from CT for adult and pediatric patients. Phys Med Biol 2015;60(14):5601–25. https://doi.org/10.1088/0031-9155/60/14/5601.

[39] Myronakis M, Stratakis J, Damilakis J. Rapid estimation of patient-specific organ doses using a deep learning network. Med Phys 2023;50(11):7236–44. https://doi.org/10.1002/mp.16356.

[40] Wasserthal J, Breit HC, Meyer MT, Pradella M, Hinck D, Sauter AW, et al. Total segmentator: robust segmentation of 104 anatomical structures in CT images. Radiol Artif Intell 2023;5:5. https://doi.org/10.1148/ryai.230024.

[41] Sánchez-Nieto B, Lopez-Martínez IN, Rodríguez-Mongua JL, Espinoza I. A simple analytical model for a fast 3D assessment of peripheral photon dose during coplanar isocentric photon radiotherapy. Front Oncol 2022;12:872752. https://doi.org/10.3389/fonc.2022.872752.

[42] Marchant T, Koshi K. Comprehensive Monte Carlo study of patient doses from cone-beam CT imaging in radiotherapy. J Radiol Prot 2017;37(1):13–30. https://doi.org/10.1088/1361-6498/37/1/13.

[43] Ardenfors O, Dasu A, Lillhök J, Persson L, Gudowska I. Out-of-field doses from secondary radiation produced in proton therapy and the associated risk of radiation-induced cancer from a brain tumor treatment. Phys Med 2018;53: 129–36. https://doi.org/10.1016/j.ejmp.2018.08.020.

[44] Romero-Expósito M, Liszka M, Christou A, Toma-Dasu I, Dasu A. Range shifter contribution to neutron exposure of patients undergoing proton pencil beam scanning. Med Phys 2023:1–10. https://doi.org/10.1002/mp.16897.

[45] Werner CJ et al. MCNP User's Manual - Code Version 6.2. Los Alamos National Laboratory, report LA-UR-17-29981. 2017.

[46] Sáez-Vergara JC, Romero AM, Ginjaume M, Ortega X, Miralles H. Photon energy response matrix for environmental monitoring systems based on LiF:Mg,Ti and hypersensitive phosphors (LiF:Mg,Cu,P and a-Al2O3:C). Radiat Prot Dosimetry 1999;85(1–4):207–11. https://doi.org/10.1093/OXFORDJOURNALS.RPD.A032835.

[47] Duggan L, Hood C, Warren-Forward H, Haque M, Kron T. Variations in dose response with x-ray energy of LiF:Mg,Cu,P thermoluminescence dosimeters: implications for clinical dosimetry. Phys Med Biol 2004;49:3831–45. https://doi.org/10.1088/0031-9155/49/17/001.

[48] De Saint-Hubert M, Boissonnat G, Schneider U, Bäumer C, Verbeek N, Esser, et al. Complete patient exposure during paediatric brain cancer treatment for photon and proton therapy techniques including imaging procedures. Front. Oncol. 2023; 13:1222800. https://doi.org/10.3389/fonc.2023.1222800.

[49] Lee H, Shin J, Verburg JM, Bobić M, Winey B, Schuemann J, et al. MOQUI: an open-source GPU-based Monte Carlo code for proton dose calculation with efficient data structure. Phys Med Biol 2022;67:174001. https://doi.org/10.1088/1361-6560/ac8716.

[50] Schneider U, Hälg RA, Lomax T. Neutrons in active proton therapy: parameterization of dose and dose equivalent. Z Med Phys 2017;27:113–23. https://doi.org/10.1016/j.zemedi.2016.07.001.

[51] Gallagher K, Taddei P. Analytical model to estimate equivalentdose from internal neutrons in proton therapy of children withintracranial tumors. Radiat Prot Dosim 2019;183:460–8. https://doi.org/10.1093/rpd/ncy166.

[52] Ding A, Gu J, Trofimov AV, Xu XG. Monte Carlo calculation of imaging doses from diagnostic multidetector CT and kilovoltage cone-beam CT as part of prostate cancer treatment plans. Med Phys 2010;37(12):6199–204. https://doi.org/10.1118/1.3512791.

[53] Choi C, Yeom YS, Lee H, Han H, Shin B, Nguyen TT, et al. Body-size-dependent phantom library constructed from ICRP mesh-Type reference computational phantoms. Phys Med Biol 2020;65(12):125014. https://doi.org/10.1088/1361-6560/ab8ddc.

[54] Kollitz E, Han H, Kim CH, Pinto M, Schwarz M, Riboldi M, et al. A patient-specific hybrid phantom for calculating radiation dose and equivalent dose to the whole body. Phys Med Biol 2022;67(3). https://doi.org/10.1088/1361-6560/ac4738.

[55] Hauri P, Radonic S, Vasi F, Ernst M, Sumila M, Mille MM, et al. Development of whole-body representation and dose calculation in a commercial treatment planning system. Z Med Phys 2022;32(2):159–72. https://doi.org/10.1016/j.zemedi.2021.05.001.

[56] Kuzmin GA, Mille MM, Jung JW, Lee C, Pelletier C, Akaban G, et al. A novel method to extend a partial-body CT for the reconstruction of dose to organs beyond the scan range. Radiat Res 2018;189(6):618–26. https://doi.org/10.1667/RR14999.1.
[57] Sánchez-Nieto B, Romero-Expósito M, Terrón JA, Irazola L, García-Hernández MT, Mateos JC, et al. External photon radiation treatment for prostate cancer: uncomplicated and cancer-free control probability assessment of 36 plans. Phys Med 2019;66:88–96. https://doi.org/10.1016/j.ejmp.2019.09.076.
[58] Harrison RM, Wilkinson M, Shemilt A, Rawlings DJ, Moore M, Lecomber AR. Organ doses from prostate radiotherapy and associated concomitant exposures. Br J Radiol 2006;79(942):487–96. https://doi.org/10.1259/bjr/16187818.
[59] Newhauser W, Fontenot J, Mahajan A, Kornguth D, Stovall M, Zheng Y, et al. The risk of developing a second cancer after receiving craniospinal proton irradiation. Phys Med Biol 2009;54:2277–91. https://doi.org/10.1088/0031-9155/54/8/002.
[60] Andrew Sa, Aird E, Shekhdar J. Contribution to normal tissue dose from concomitant radiation for two common kV-CBCT systems and one MVCT system used in radiotherapy. Radiother Oncol 2012;105(1):139–44. https://doi.org/10.1016/j.radonc.2012.04.017.
[61] Hashim S, Karim MKA, Bakar KA, Sabarudin A, Chin AW, Saripan MI, et al. Evaluation of organ doses and specific k effective dose of 64- slice CT thorax examination using an adult anthropomorphic phantom. Radiat Phys Chem 2016;126:14e20. https://doi.org/10.1016/j.radphyschem.2016.05.004.
[62] Lee C, Kim KP, Long D, Fisher R, Tien C, Simon SL, et al. Organ doses for reference adult male and female undergoing computed tomography estimated by Monte Carlo simulations. Med Phys 2011;38(3):1196–206. https://doi.org/10.1118/1.3544658.
[63] Smith-Bindman R, Wang Y, Chu P, Chung R, Einstein AJ, Balcombe J, et al. International variation in radiation dose for computed tomography examinations: prospective cohort study. BMJ 2019 Jan;2(364):k4931. https://doi.org/10.1136/bmj.k4931.
[64] Bolsi A, Peroni M, Amelio D, Dasu A, Stock M, Toma-Dasu I, et al. Practice patterns of image guided particle therapy in Europe: a 2016 survey of the European Particle Therapy Network (EPTN). Radiother Oncol 2018;128(1):4–8. https://doi.org/10.1016/j.radonc.2018.03.017.